ELSEVIER

Thermochimica Acta 256 (1995) 75–89

thermochimica acta

Thermal analysis as an aid in the synthesis of non-stoichiometric perovskite type oxides ☆

H. Fjellvåg *, O.H. Hansteen, B.G. Tilset, A. Olafsen, N. Sakai [1], H. Seim

Department of Chemistry, University of Oslo, Box 1033 Blindern, N-0315 Oslo, Norway

Abstract

The controlled synthesis of non-stoichiometric perovskite type oxides is of importance for fundamental and applied studies. The present contribution focuses on how data from thermal analysis, mainly thermogravimetry and X-ray powder diffraction, can be utilized for defining optimum synthesis conditions. The perovskite oxides frequently have (or are formed from binary oxides with) high stability and low reactivity. The synthesis of a homogeneous and pure reaction product is limited by diffusion controlled mass transport, and precursor materials with mixing of cations on a microscopic level are therefore needed. The decomposition of citrate precursors, the formation and decomposition of intermediates, the control of oxygen non-stoichiometry, the decomposition of the product and reactions/phase transitions on cooling are considered. As examples, thermal analysis data are provided and discussed for major steps in the syntheses of non-stoichiometric $LaMO_3$ (M is V, Cr, Mn, Fe, Co or Ni).

Keywords: Lanthanum compound; Mixed oxide; Non-stoichiometric; Perovskite; TG

1. Introduction

$REMO_3$ (RE is a 4f element, M is a 3d element) perovskite type related phases, including substituted variants, are of potential use as materials in cathodes and

☆ Presented at the 14th Symposium on Thermal Analysis and Calorimetry, Oslo, Norway, 15–17 June 1994.

* Corresponding author.

[1] Permanent address: Department of Inorganic Materials, National Institute of Materials and Chemical Research, 1-1 Higashi, Tsukuba, Ibaraki 305, Japan.

SSDI 0040-6031(94)02220-8

interconnects in solid oxide fuel cells, as oxygen sensors or as catalysts [1,2]. In this respect, a knowledge of correlations between composition, atomic arrangement and physical and chemical properties is of great importance, in particular at operating conditions. A prerequisite for detailed property studies is the controlled synthesis of materials with specified composition, with respect to both aliovalent substitutions and oxygen non-stoichiometry. Thermal analyses by means of diffraction and thermogravimetric methods are powerful tools to aid in defining optimal synthesis conditions.

Several $REMO_3$ perovskite type oxides have (or are formed from binary oxides with) low reactivities and high decomposition temperatures [2,3]. Problems which are encountered in the synthesis of such phases or solid solution variants have their origin in the particle size of the reactants, which leads to long reaction times (more reaction cycles) for diffusion controlled mass transport at moderate temperatures and possible contamination from the crucible if too high a temperature is adopted. A controlled synthesis of pure and homogeneous products calls for methods by which mixing at an atomic level is assured in the precursor materials.

In relation to property studies, there is a need to monitor and control the oxygen non-stoichiometry (y or δ for $REMO_{3-y}$ or $REMO_{3+\delta}$) during synthesis. The dominating defects are typically vacancies at the O site [4–6], frequently associated into defect clusters. For a few perovskites, among them $LaMnO_{3+\delta}$ [6], substantial oxygen excess occurs, which notably is not brought about by oxygen interstitials, but rather by large numbers of metal atom vacancies [6]. The perovskite type oxides considered here are described by the general formula $(RE_{1-x}M)_{1-z}O_{3-y}$, where ideally x, y and z are zero.

Several perovskite materials exhibit drastic variations in properties on changes in the oxygen non-stoichiometry [7,8]. During the final stage of the synthesis, the non-stoichiometry can be adjusted through appropriate choices of temperature and oxygen partial pressure conditions. However, the oxygen content and its distribution within the sample are significantly influenced by conditions during the final cooling. For materials of potential practical use, the complexity may even be higher than that described here, usually owing to aliovalent substitutions, as in such solid solution phases as $La_{1-x}AE_xCrO_{3-y}$ [9] (AE is an alkaline earth) and $La_{1-x}Sr_xMnO_{3-y}$ [10].

Thermogravimetric analysis and X-ray powder diffraction may provide information on crucial aspects of the perovskite synthesis, including the decomposition of precursors, the formation and decomposition of intermediate phases, the oxygen stoichiometry of the final product, decomposition of the products in reducing atmospheres, decomposition of products during cooling from the reaction conditions, and temperature induced phase transitions.

Attention at present is focused on important steps in the synthesis of $LaMO_3$ (M is V, Cr, Mn, Fe, Co or Ni), from precursor via intermediates to a final oxide, with a specific oxygen non-stoichiometry (y, δ). The examples provided demonstrate how thermal analysis data may help define and optimize synthesis conditions for $REMO_{3-y}$.

2. Experimental

2.1. Syntheses from citrate solutions

The starting materials for the syntheses were La_2O_3 (99.98%, Fluka; 99.9%, Aldrich; 99.99%, Molycorp), V_2O_5 (99.5%, Riedel de Häen AG), CrO_3 (> 99%, Merck), $Mn(CH_3COO)_2 \cdot 4H_2O$ (> 99%, Fluka), $Co(CH_3COO)_2 \cdot 4H_2O$ (> 99%, Fluka), $Ni(CH_3COO)_2 \cdot 4H_2O$ (> 99%, Fluka) and citric acid monohydrate $C_3H_4(OH)(COOH)_3 \cdot H_2O$ (reagent grade, Sturge Biochemicals). The detailed synthesis procedure was slightly different for the various La–M–O systems. In general, La_2O_3 was stirred with citric acid monohydrate in about 1:(30–50) ratio by weight, with a few droplets of water added. The La_2O_3 dissolved in the melt during heating to 420–450 K and a clear solution was obtained. The 3d metal component was then added along with additional water. The citrate solution was dehydrated at 450 K, forming first a polymer gel and finally a porous, X-ray amorphous xerogel. Most of the carbonaceous species were subsequently removed by incineration at 620–720 K. The finely crushed powder was pressed into pellets, placed in alumina crucibles and fired in air or pure oxygen, typically at 1070–1270 K for 24 h. The samples were then crushed, pelletized and subjected to one similar heat treatment before the oxygen content, if required, was monitored during a final heat treatment.

The $La_{1-x}MnO_{3-y}$ samples, studied here with respect to non-stoichiometry, were prepared from mixtures of titrated aqueous solutions of $LaCl_3$ and $MnCl_2$. Addition of ammonium carbonate forced the precipitation of $La_2(CO_3)_3$ and $MnCO_3$. After drying and washing, the carbonate mixture was calcined at 1373 K to provide a single phase oxide. The oxygen content was monitored in a final heat treatment.

2.2. Monitoring of oxygen content

Based on literature data and on results from thermal analysis (see below), the appropriate atmospheric conditions were selected in order to obtain the desired oxygen stoichiometry of the products. The final heat treatments were performed either in a TG apparatus or in tube furnaces at temperatures between 800 and 1850 K. A similar set-up for gas mixing and measurement of oxygen potential, see Fig. 1, was adopted for controlled synthesis and for thermogravimetric and X-ray powder diffraction studies. Moderate to high oxygen partial pressures were obtained by mixing oxygen and argon, their relative amounts being regulated by flowmeters. Low oxygen partial pressures, $p(O_2) < 10^2$ Pa, were obtained in $H_2/CO_2/Ar$ gas mixtures. The actual oxygen potentials were monitored by oxygen sensors (electrochemical sensors based on Y-stabilized zirconia; PBI-Dansensor, types HT and TIA-222-II for the synthesis equipment; home-made sensors for the TG and XPD equipment; air acting as reference) with a cell voltage

$$E = \frac{RT}{4F} \ln\left[\frac{p(O_2)_{ref}}{p(O_2)}\right]$$

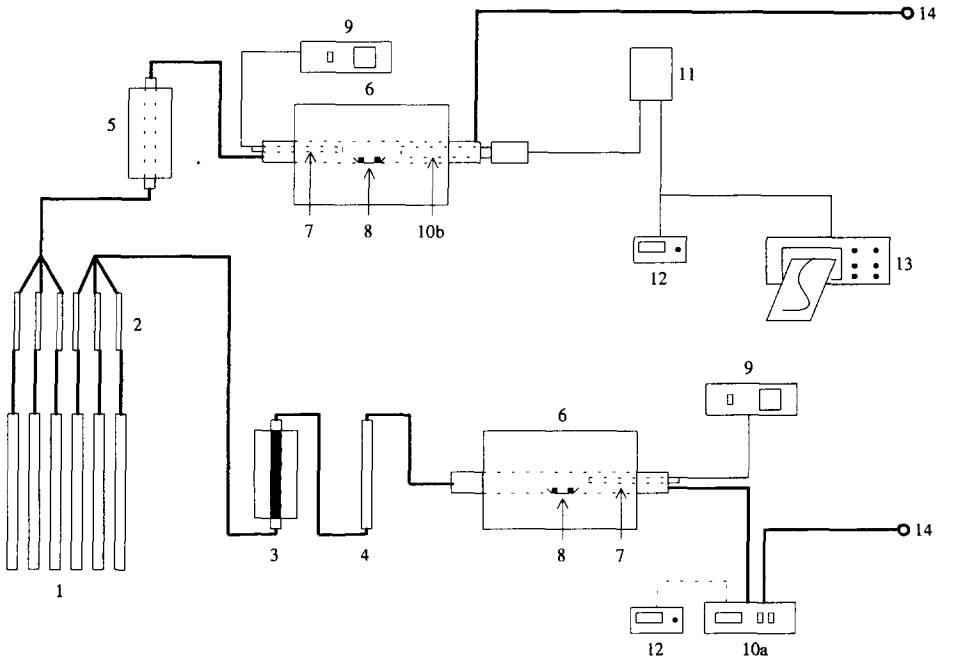

Fig. 1. Flow sheet for equipment used for synthesis in a controlled atmosphere. The main features concerning gas mixing and gas analysis are the same for equipment used in materials synthesis, TG analysis and XPD studies in controlled atmospheres. 1, gas bottles; 2, flowmeters; 3, furnace; carbon oxidation; 4, drying column; KOH; 5, gas mixing; 6, tube furnace; alumina tubes; 7, thermocouple; 8, alumina crucible; 9, temperature controller; 10, oxygen sensor; 11, signal receiver; 12, voltmeter; 13, plotter; 14, gas outlet.

CO/CO_2 mixtures were avoided owing to problems with carbon deposition. In the case of $H_2/CO_2/Ar$ gas mixtures, simultaneous equilibria were considered during calculations of the oxygen partial pressure. For this purpose the SOLGAS [11], GEM [12] and STELLA [13] programs were used.

Measurements on certificated O_2/inert gas mixtures show that the lower limit for the attainable oxygen partial pressure in the synthesis furnace is 1–10 Pa. The limit is dictated by impurities in the source gases and by leakages. For the $H_2/CO_2/Ar$ gas mixtures with $p(O_2) < 1$ Pa, the reasonable agreement between calculated and measured oxygen partial pressures (e.g., observed 4.3×10^{-10}, calculated 6.5×10^{-10} Pa) indicated that the buffered gas system was close to equilibrium.

2.3. Characterization

The intermediate phases and the reaction products were characterized by room temperature X-ray powder diffraction XPD (Guinier–Hägg cameras, Cu $K\alpha_1$ and Cr $K\alpha_1$ radiation, Si as internal standard). Information was thereby obtained on the crystallinity, phase content and homogeneity of reaction products at different stages

during the syntheses. The detection limit for possible impurity phases was established from mechanical two-phase mixtures.

High temperature X-ray powder diffraction data were collected in two ways. A Guinier Simon camera (Enraf Nonius) was used for temperatures between 300 and 1200 K. The samples were kept in rotating, sealed or open quartz capillaries, and the temperature change was synchronized with the movement of a film cassette (the detector). The temperature was calibrated via measurements of the thermal expansion of silver [14]. The diffraction patterns on the film provide a two-dimensional visualization (temperature versus scattering angle) of changes connected with reactions, crystallization, decompositions or phase transitions.

A Siemens D500 diffractometer with high temperature attachment was used for studies in a controlled atmosphere. The powder sample was placed on a Pt heating filament. The oxygen partial pressure of the flowing gas surrounding the sample was monitored by an O_2 sensor positioned in a separate oven. The temperature close to the sample position on the filament was measured by a Pt–13%Rh (type R) thermocouple.

Thermogravimetric analysis (TGA) and differential thermal analysis (DTA) were performed with Perkin-Elmer TGA7 and DTA7 instruments. Several TGA experiments were stopped at stages considered to be representative of the thermal decomposition, reduction and oxidation reactions, and samples were withdrawn for examination by XPD at room temperature. Attempts were made to reproduce the T, $p(O_2)$ conditions for phase stability established in the TGA experiments during synthesis and in-situ diffraction experiments.

3. Results and discussion

3.1. Decomposition of citrate precursors

In air, the RE–M citrate gels start to decompose between 470 and 570 K; see the TGA data for a La–Ni–citrate precursor in Fig. 2. The product at 700 K is in general X-ray amorphous. For most La–M–O systems, the weight loss observed on further temperature increase indicates that RE oxide carbonates predominate as intermediate phases. The formation of such intermediates and their subsequent decomposition into the desired products depend strongly on the CO/CO_2 content of the surrounding atmosphere. The dehydrated citrate gels contain >80 wt% of organic material (see Fig. 2). Their H and O contents depend on the degree of polymerization, but are in any case lower than the ratio dictated by the anhydrous citric acid with a C:O:H molar ratio of 6:7:8.

During heating in a muffle furnace in air at 620–720 K with surplus oxygen, the precursor burns with the formation of CO_2 and H_2O. In this case, the sample is definitely subjected to a high oxygen partial pressure. On the other hand, when the incineration is conducted within a restricted volume with limited oxygen supply, as would be the case for the small open quartz capillaries used for high temperature XPD studies (typically with diameter 0.3 mm and length 20 mm), an undefined,

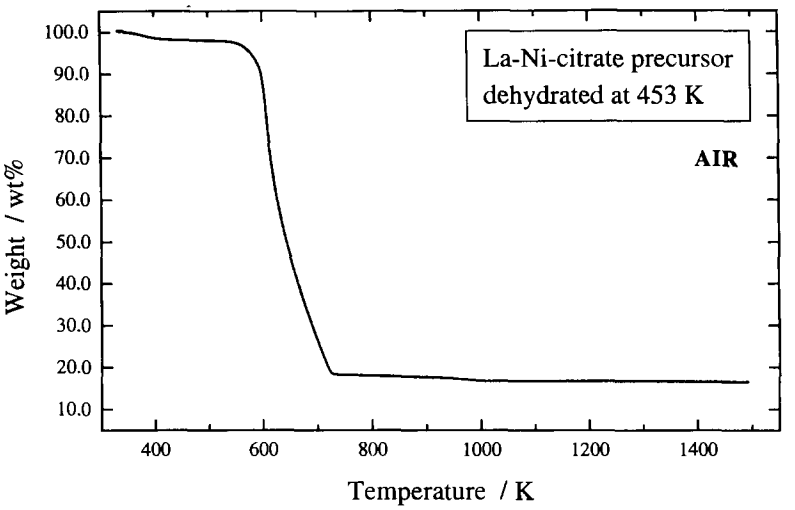

Fig. 2. Thermogravimetric data for decomposition of an amorphous La–Ni–citrate precursor on heating in air (10 K min^{-1}).

strongly reducing atmosphere results. Such possible differences in reaction conditions between different experimental set-ups must be considered when evaluating and comparing data from thermal analysis. This difference in reducing power of the atmosphere during incineration in TGA and XPD equipment can be illustrated by the La–V–O system. Thermal decomposition of a La–V–citrate xerogel during TG in air yields $LaVO_4$, independent of the original oxidation state in the citrate solution, and the $LaVO_3$ perovskite is first obtained on subsequent treatment at low oxygen partial pressures (1273 K and $p(O_2) < 10^{-7.8}$ Pa [15]). Decomposition of the precursor inside the open capillary during XPD (Guinier Simon) experiments gives crystalline $LaVO_3$ directly [16].

The large effective CO/CO_2 partial pressure inside the XPD capillaries affects also the thermal decomposition of the simple La–citrate xerogels, where no such redox reactions take place. In XPD studies (open capillaries), $La_2O_2CO_3$ is the reaction product at 1133 K, whereas TGA experiments in flowing air give La_2O_3 at the same temperature. The observations may be understood by considering the equilibrium

$$La_2O_2CO_3(s) \rightarrow La_2O_3(s) + CO_2(g) \quad K = p(CO_2)$$

The oxide carbonate formation depends on the precursor material (citrate, acetate or oxalate). The $La_2O_2CO_3$ modifications (I, IA and II) decompose under different conditions spanning an interval of more than 200 K in air [17–19]. The TGA data in Fig. 3 show that, in pure CO_2, the last step in the decomposition of the La–citrate precursor from $La_2O_2CO_3$ to La_2O_3 occurs around 1225 K [20]. Similar behaviour is found for $Nd_2O_2CO_3$, which, according to XPD, is of type II prior to the decomposition. In this way, combined TGA and XPD data help in defining conditions for the preparation of crystalline oxide carbonates [20].

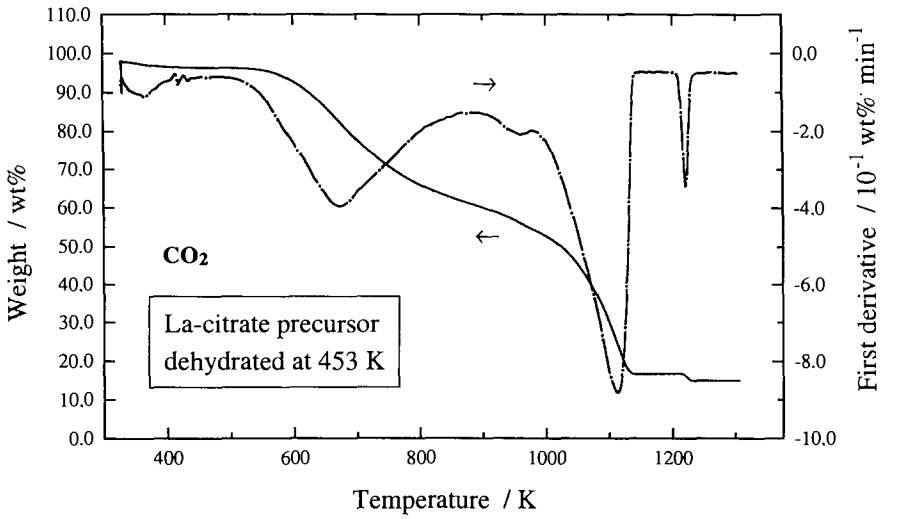

Fig. 3. Thermogravimetric data for decomposition of amorphous La-citrate precursor via $La_2O_2CO_3$ to La_2O_3 on heating in air (10 K min^{-1}).

3.2. Characterization of reaction intermediates and products

The amorphous or poorly crystalline material obtained after incineration in air at 650–700 K is pelletized and calcined. During the calcination in a CO_2-containing atmosphere (e.g., air with 0.03% of CO_2), any basic cations present will be susceptible to carbonatization reactions competing with oxide formation. It is necessary to select conditions under which either carbonate formation is impossible (e.g. by using carbon-free precursors and atmospheres [21]) or carbonates are unstable [22].

The synthesis of $LaNiO_3$ represents a rather complex reaction sequence, where the xerogel decomposes into a multiphase mixture during the incineration and calcining steps [23]. First, poorly crystalline $La_2O_2CO_3$ (modification I) is formed together with NiO at $\sim$673 K. Then $La_2O_2CO_3$ (I) decomposes into La_2O_3 and CO_2 around 925 K (Fig. 4). The obtained La_2O_3, probably with a large surface area, reacts with NiO with the formation of $LaNiO_3$ (the desired product) and La_2NiO_4. This is indicated by the weight increase in Fig. 4 above 1070 K. XPD shows that the reaction product after cooling from 1300 K is a multiphase, non-equilibrium mixture of La_2NiO_4, $La_4Ni_3O_{10}$, La_2O_3 and NiO. The weight reduction at the highest temperatures in Fig. 4 corresponds to oxygen loss on reduction of Ni(III).

With the reaction complexity in mind, it is desired to define conditions where, e.g., $LaNiO_3$ and $La_4Ni_3O_{10}$ can conveniently be obtained in the pure state. Based on thermal analysis data (Fig. 5) and estimations of phase stability as a function of temperature and oxygen partial pressure [24], the maximum heat treatment temperature is considered to be $\sim$ 1123 K in oxygen (10^5 Pa). The weight loss observed by

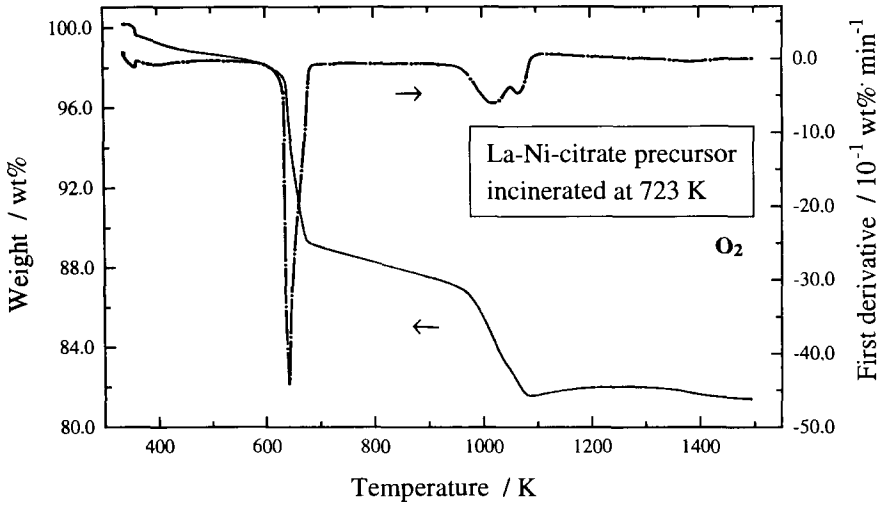

Fig. 4. Thermogravimetric data for decomposition of amorphous/poorly crystalline La–Ni precursor containing $NiO/La_2O_2CO_3$ precursor on heating in oxygen (10 K min^{-1}).

TGA gives an average oxygen content corresponding to $LaNiO_{2.72}$ at 1473 K. XPD indicates that the reaction

$$4LaNiO_3(s) \rightarrow La_4Ni_3O_{10}(s) + NiO(s) + 0.5O_2(g)$$

is taking place. The polyphasic solid product has an average oxygen content of $LaNiO_{2.75}$. $La_4Ni_3O_{10}$ tends to decompose further.

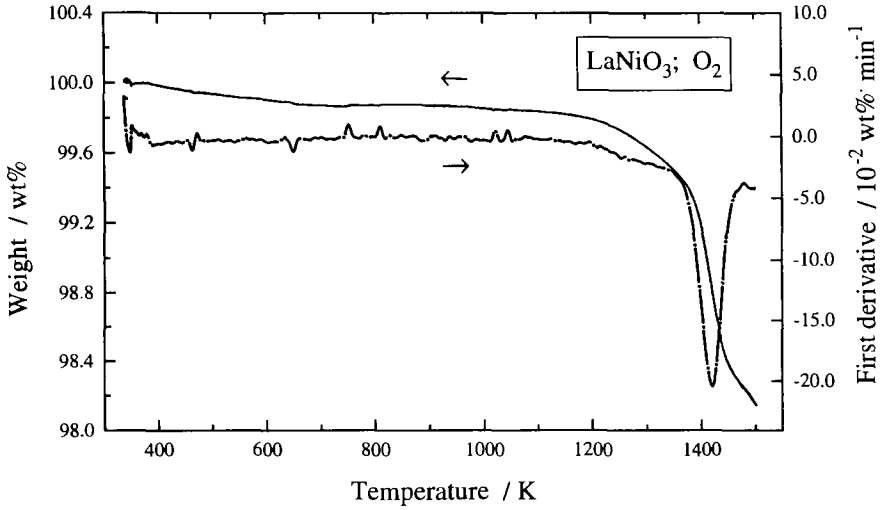

Fig. 5. Thermogravimetric data for decomposition of $LaNiO_3$ on heating in oxygen (10 K min^{-1}).

In some La–M–O systems, the intermediates do not cause inhomogeneity problems as represented and described for La_2NiO_4 above. During preparation of $LaCrO_3$ by the citric acid method, the pentavalent chromium compound $LaCrO_4$, with the same La/Cr ratio as the desired product, is formed during the incineration. No major formation of oxide carbonates occurs. $LaCrO_4$ is formed irrespective of whether Cr(III) or Cr(VI) is present in the reactants. When Cr(VI) is added to citric acid, a reduction of chromium occurs along with oxidative decomposition of the acid. When Cr(III) is present in the citric acid, incineration in air at ~ 700 K apparently causes oxidation to Cr(V). $LaCrO_4$ decomposes to $LaCrO_3$ on heating [24–27]. Whereas $LaCrO_4$ forms easily from the precursor on incineration, no $LaCrO_4$ could be obtained on heating $LaCrO_3$ in air at 723 K for 6 days [28].

3.3. Control of oxygen non-stoichiometry

Oxygen non-stoichiometry in $REMO_3$ implies either oxygen deficiency or oxygen excess. First, oxygen vacancy formation is considered. At high temperatures, substantial non-stoichiometry is intrinsic to $REMO_{3-y}$ materials and represents a stable situation thermodynamically. The non-stoichiometry is defined by temperature and oxygen partial pressure

$$REMO_3(s) \rightarrow REMO_{3-y}(s) + (y/2)O_2(g)$$

and defect clusters M(II)–vacancy–M(II) are considered to occur [5].

A representative, schematic phase diagram for $REMO_{3-y}$ is shown in Fig. 6. The same composition $(3-y)$ may be achieved for different choices of temperature and partial pressure. In Fig. 6, the existence of two modifications separated by a first order transition is anticipated. This situation is relevant for, e.g. $La_{1-x}Ca_xCrO_3$ and $LaMnO_{3+\delta}$, where rhombohedral and orthorhombic variants of the perovskite type structure exist.

During the synthesis steps considered so far, efforts were made to obtain a phase pure product which can be used as the starting material for controlled reductions. Note that such starting materials do not necessarily have the maximum possible oxygen content for the actual phase. Higher oxygen contents may possibly be attained via high pressure or electrochemical methods [29,30]. In the following, emphasis is put on reduced oxides. By monitoring the non-stoichiometry, the physical properties may be tailored. $YBa_2Cu_3O_{7-\delta}$ provides a striking example, being a semiconducting antiferromagnet for $\delta \approx 1$ and a high-T_c superconductor for $\delta \approx 0$ [8].

The maximum attainable equilibrium non-stoichiometry is strikingly different among $REMO_{3-y}$. $LaCrO_3$ has no tendency towards oxygen non-stoichiometry [31]. $LaCoO_{3-y}$, on the other hand, can easily be reduced and the phase extends over a significant composition interval (say $y < 0.10$) at high temperatures [32]. When M is Mn, the material synthesized in air has oxidative non-stoichiometry, $LaMnO_{3+\delta}$ (up to 40% of Mn(IV) by high pressure methods [7]). On reduction, Mn(IV) is converted into Mn(III), and under strongly reducing conditions oxygen vacancies may even occur, $LaMnO_{3-y}$ [33].

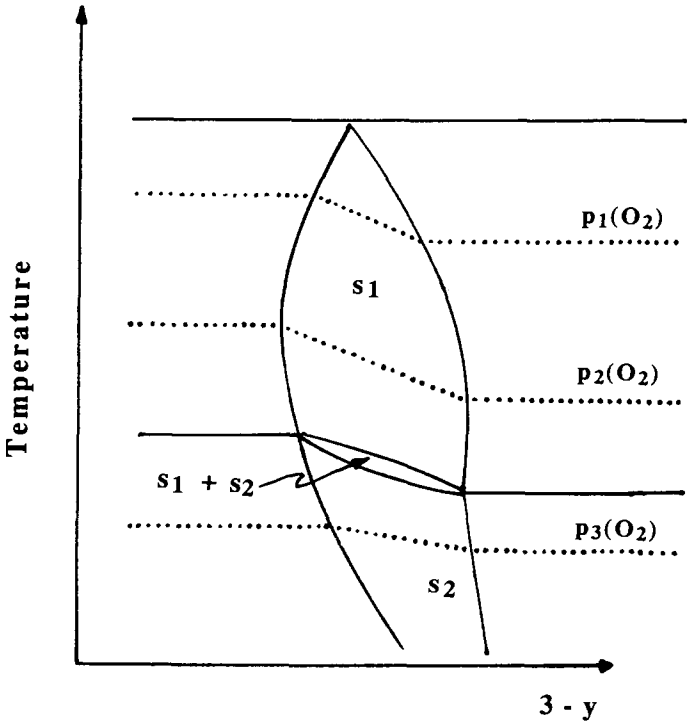

Fig. 6. Schematic temperature, composition phase diagram for non-stoichiometric $LaMO_{3\pm y}$. The $LaMO_{3\pm y}$ is assumed to exist in two polymorphic forms separated by a first-order structural phase transition. Equilibrium situations for three oxygen partial pressures are indicated.

At low temperatures, the intrinsic oxygen non-stoichiometry tends to decrease. Nevertheless, it is possible at low temperatures (say $T < 700$ K) to obtain a huge oxygen deficiency [34]. The low temperature reduced phases are usually metastable. The La–Co–O phase diagram predicts La_2CoO_4 + CoO as the stable situation when La:Co = 1:1, $T = 1273$ K and $p(O_2) = 1.8 \times 10^{-2}$ Pa [35]. However, on reducing $LaCoO_3$ at, say, 700 K, the processes involving breaking of bonds, nucleation and growth of the new phases are slow. Instead of the formation of the stable phases, the basic perovskite type atomic arrangement is retained and oxygen atoms are removed in a topotactic reaction. In this way, $LaCoO_3$ is reduced to $LaCoO_{2.5} = La_2Co_2O_5$ with a Brownmillerite related superstructure [36].

The reduction can be performed in various more or less controlled ways. A sequence of phase stabilities can straightforwardly be traced by passing hydrogen, or a strongly reducing gas mixture, over the sample [36] while observing weight changes by TGA or H_2 consumption by TPR. The reduction goes normally through several steps. When, e.g., M is Co or Ni, the final product is metal on RE_2O_3. In a repeated experiment, specimens were taken at different, representative stages of the reduction and characterized. In this way, TPR was used to define experimental conditions for the reduction of $LaCo_{1-t}Cr_tO_3$ (with Co(III)) to $LaCo_{1-t}Cr_tO_{3-t/2}$

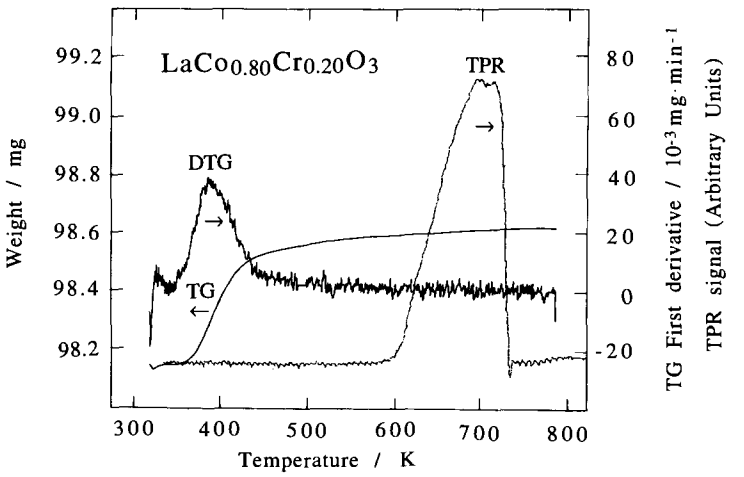

Fig. 7. Reduction of $LaCo_{0.80}Cr_{0.20}O_3$ in flowing hydrogen (10%) during TPR experiments, and reoxidation during TG experiments after handling in air.

(with Co(II)) [18]; see Fig. 7. The reduced phase obtained in a topotactic reaction at $T < 750$ K is probably metastable.

A different approach is to extract oxygen from $REMO_3$ by oxidizing weighed amounts of zirconium metal, which is positioned in a separate crucible during the annealing but within the same sealed and evacuated silica glass ampoule [16,23]. Zr, under quantitative formation of ZrO_2, was successfully used for reducing $LaCoO_3$ to $La_2Co_2O_5$ [23], and $LaVO_4$ to $LaVO_3$ [16]. The TGA reoxidation curve for

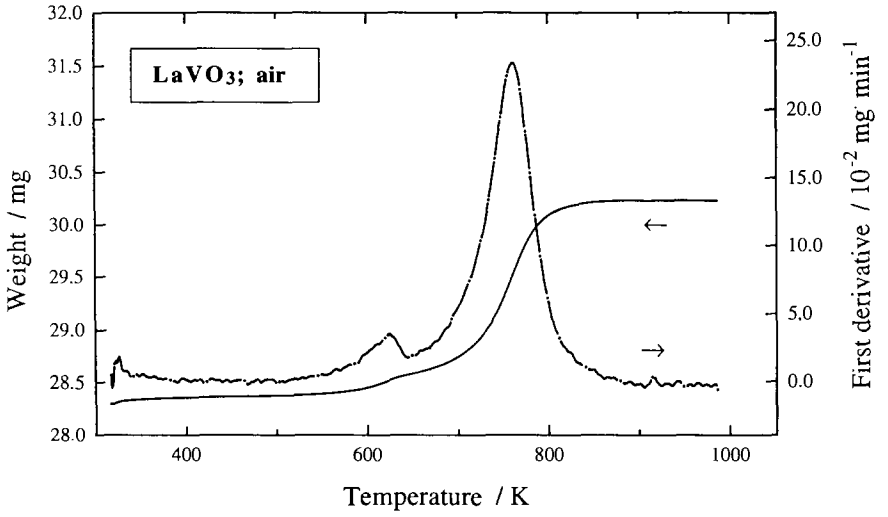

Fig. 8. Reoxidation of $LaVO_3$ in air on heating to 973 K (heating rate 10 K min^{-1}).

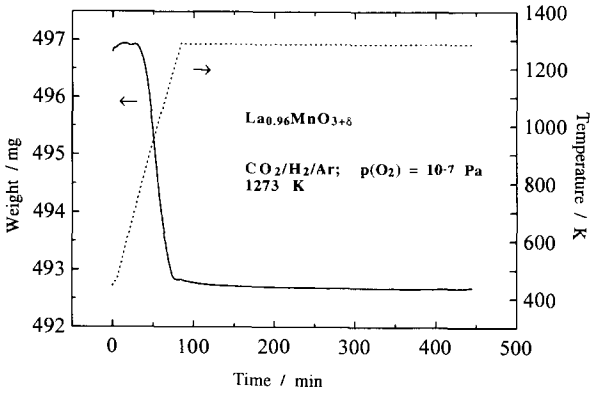

Fig. 9. Time evolution of the reduction of $La_{0.96}MnO_{3+\delta}$ in a $CO_2/H_2/Ar$ gas mixture with $p(O_2) = 10^{-7}$ Pa at $T = 1273$ K.

$LaVO_3$ is shown in Fig. 8. $LaVO_3$ is first oxidized continuously to $LaVO_{3.12}$, and thereafter $LaVO_4$ is formed [16].

A third, and more controlled, way of reduction is to equilibrate the sample under defined temperature and partial pressure conditions and thereby obtain the non-stoichiometry predicted by the equilibrium phase diagram (see Fig. 6). The TGA apparatus itself is an excellent tool for such experiments. On reduction of $La_{0.96}MnO_{3+\delta}$ in a $CO_2/H_2/Ar$ mixture with $p(O_2) = 10^{-7}$ Pa at 1273 K, constant weight corresponding to $La_{0.96}MnO_{2.94}$ is achieved after 200 min (Fig. 9) with solely trivalent manganese. On subsequent heating in oxygen (20 ml min^{-1}), $La_{0.96}MnO_{2.94}$ starts to reoxidize at 750 K (Fig. 10). On subsequent slow cooling to room temperature a further weight gain occurs, see Fig. 10.

The structural closeness of the oxidized and reduced (partly metastable) perovskites facilitates easily reoxidation, which is an obstacle for the controlled synthesis, handling and property studies. The affinity towards reoxidation is strik-

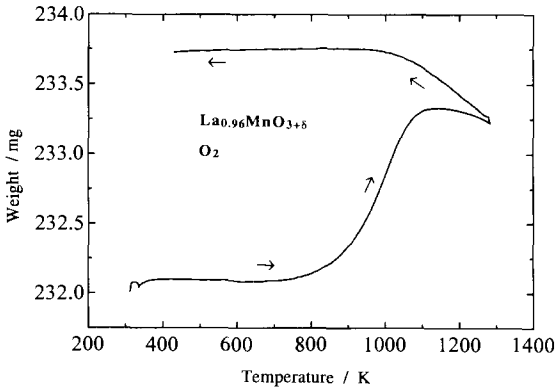

Fig. 10. Reoxidation of $La_{0.96}MnO_{2.94}$ in O_2 on heating to 1273 K (heating rate 10 K min^{-1}) and on subsequent cooling in O_2 to room temperature.

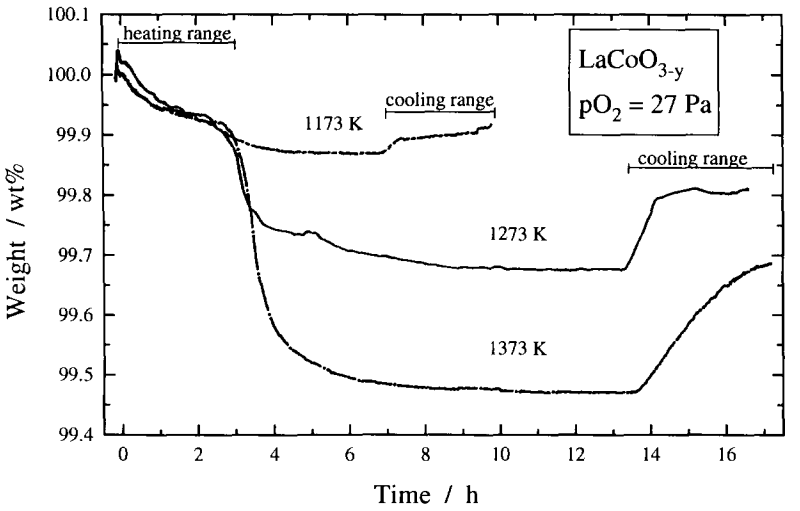

Fig. 11. Reduction of $LaCoO_{3-y}$ in flowing nitrogen with $p(O_2) = 27$ Pa at 1173, 1273 and 1373 K and subsequent reoxidation on cooling (5 K min^{-1}) to room temperature.

ingly different among the La–M–O systems. According to TGA experiments [37], $LaMnO_3$ starts to reoxidize to $LaMnO_{3.15}$ at ~ 750 K (pure O_2, heating rate 10 K min^{-1}, gas flow 20 ml min^{-1}), $LaVO_3$ starts to reoxidize to $LaVO_{3.12}$ at ~ 600 K (heating rate 10 K min^{-1}) [16], but $LaCoO_{3-y}$ has started to reoxidize to $LaCoO_3$ already at 350 K (heating rate 5 K min^{-1}) [23]. However, for many samples the situation is even worse. $LaCo_{0.80}Cr_{0.20}O_{2.58(2)}$ is oxidized to $LaCo_{0.80}Cr_{0.20}O_{2.93(1)}$ at 298 K during a couple of days [28]. It is worth noting that the reoxidation occurs at a substantially higher temperature for $LaMnO_{3+\delta}$ than for $LaCoO_{3-y}$, which probably indicates that for $LaCoO_{3-y}$ oxygen vacancies prevail, whereas for $LaMnO_{3+\delta}$ the non-stoichiometry involves vacancies at the RE and M sites [6].

3.4. Decomposition on cooling

The cooling of a non-stoichiometric $REMO_{3-y}$ sample equilibrated in a reducing atmosphere is associated with several problems. The non-stoichiometry is generally temperature dependent (see Fig. 6). The sample to be studied at ambient temperature may represent (i) a frozen, metastable defect situation at some rather undefined conditions at elevated temperature, (ii) an equilibrium one-phase situation maintained during the entire cooling (which in practice can hardly be achieved), or (iii) a non-equilibrium situation where the sample is partly decomposed into other stable compounds. In practice, it is hard to differentiate between these cases.

The situation (iii) is illustrated by $LaCoO_{3-y}$. Fig. 11 shows TGA reduction curves for $LaCoO_{3-y}$ in a flowing N_2 atmosphere with $p(O_2) = 27$ Pa at $T = 1173$, 1273, and 1373 K. The oxygen partial pressure is within the stability domain of the non-stoichiometric phase, and equilibrium (constant weight) is achieved within 5–15 h. A weight increase occurs on cooling and indicates the partial reoxidation

of $LaCoO_{3-y}$. Subsequent XPD at 300 K for the sample equilibrated at 1373 K shows $LaCoO_3$ and $La_4Co_3O_{10}$ (some CoO or Co_3O_4 ought to be present, but is not observed). This shows that, when the non-stoichiometry is large, the oxygen supply is limited and the cooling rate is substantial, and the sample does not equilibrate completely during cooling. The non-stoichiometry then exceeds the stability limit of $LaCoO_{3-y}$ and disproportionation occurs

$$LaCoO_{3-y} \rightarrow (1-a)LaCoO_{3-y} + a/4(La_4Co_3O_{10} + (1/3)Co_3O_4)$$

3.5. Effect of first-order phase transitions

Some $REMO_{3-y}$ undergo phase transitions as a function of temperature and oxygen partial pressure. This complicates structure – property considerations, as the crystal structure at ambient temperature, which forms the natural basis, may be inadequate for the high temperature situation. Comparison of data from in-situ experiments and quenched samples will tell whether transitions occur. The cooling/quenching rate in the final step of the synthesis may be too fast for nucleation and growth of the low temperature phase, and the equilibrium oxygen content may be different for the two phases.

For $La_{1-x}MnO_{3+\delta}$, three differently deformed phases occupy distinct regions in the T, $p(O_2)$ phase diagram constructed on the basis of XPD data for quenched samples. In-situ experiments convey, however, a quite different picture [37]. $La_{0.96}MnO_{2.94}$ quenched from $T = 1073$ K and $p(O_2) = 10^{-7}$ Pa is orthorhombic, whereas in situ experiments at the same T, $p(O_2)$ conditions show a rhombohedral phase [37]. The first-order phase transition between the orthorhombic and rhombohedral modifications occurs at ~ 650 K [$p(O_2) = 10^{-7}$ Pa]. On quenching, structural rearrangement does occur, which seems reasonable, because breaking of bonds and mass diffusion is not involved, solely a change in the tilting of the coordination polyhedra. The quenched sample represents in this case the stable situation at 300 K, but does not give the correct picture of the crystal structure under the quenching conditions.

4. Conclusions

Thermal analyses by means of TG and XPD under controlled atmosphere conditions are important tools for selecting appropriate synthesis conditions to achieve phase purity, homogeneity and the desired non-stoichiometry of perovskite type materials.

Acknowledgements

This work was supported financially by The Norwegian Research Council, and by Norsk Hydro A.S.

References

[1] N.Q. Minh, J. Am. Ceram. Soc., 76 (1993) 563.
[2] L.G. Tejuca and J.L.G. Fierro (Eds.), Properties and Applications of Perovskite-type Oxides, Marcel Dekker, 1992, Ch. 10–17.
[3] J.-P. Coutures, J.M. Badie, R. Berjoan, J. Coutures, R. Flamand and A. Rouanet, High Temp. Sci., 13 (1980) 331.
[4] L.G. Tejuca, J. Less-Common Met., 146 (1989) 251.
[5] J.A.M. van Roosmalen and E.H.P. Cordfunke, J. Solid State Chem., 93 (1991) 212.
[6] J.A.M. van Roosmalen and E.H.P. Cordfunke, J. Solid State Chem., 110 (1994) 109.
[7] M. Verelst, N. Rangavittal, C.N.R. Rao and A. Rousset, J. Solid State Chem., 104 (1993) 74.
[8] J.M. Tarascon, P. Barboux, P.F. Miceli, L.H. Greene, G.W. Hull, M. Eibschutz and S.A. Sunshine, Phys. Rev. B, B37 (1988) 7458.
[9] J. Mizusaki, S. Yamauchi, K. Fueki and A. Ishikawa, Solid State Ionics, 12 (1984) 119.
[10] A. Mackor, T.P.M. Koster, J.G. Kraaijkamp, J. Gerretsen and J.P.G.M. van Eijk, Proc. 2nd Int. Symp. Solid Oxide Fuel Cells, 1991, p. 463.
[11] G. Eriksen, Acta Chem. Scand., 25 (1971) 2651.
[12] T. Matsumoto, program GEM, Gibbs Energy Minimizer, Kagaku Gijutsu-Sha, Tokyo, Japan, 1992.
[13] B. Richmond, program STELLA for MacIntosh, High-Performance Systems, Hanover, USA; I. Dahl and U. Olsbye, SINTEF, Oslo, Norway, personal communication (1993); W. Tsang and R.F. Hampson, J. Phys. Chem. Ref. Data, 15 (1986) 1087.
[14] J. Spreadborough and J.W. Christian, J. Sci. Instrum., 36 (1959) 116.
[15] T. Nakamura, G. Petzow and L.J. Gauckler, Mater. Res. Bull., 14 (1979) 649.
[16] H. Seim and H. Fjellvåg, to be published.
[17] J.O. Sawyer, P. Caro and L. Eyring, Monatsh. Chem., 102 (1971) 333.
[18] R.P. Turcotte, J.O. Sawyer and L. Eyring, Inorg. Chem., 8 (1969) 238.
[19] V.V. Subba Rao, R.V.G. Rao and A.B. Biswas, J. Inorg. Nucl. Chem., 27 (1965) 2525.
[20] A. Olafsen and H. Fjellvåg, to be published.
[21] M. Karppinen, L. Niinistö and M. Véber, Acta Chem. Scand., 46 (1992) 255.
[22] H. Fjellvåg, P. Karen, A. Kjekshus, P. Kofstad and T. Norby, Acta Chem. Scand., Ser. A, A42 (1988) 178.
[23] O.H. Hansteen and H. Fjellvåg, to be published.
[24] H. Yokokawa, T. Kawada and M. Dokiya, J. Am. Ceram. Soc., 72 (1989) 2104.
[25] A. Roy and K. Nag, J. Inorg. Nucl. Chem., 40 (1978) 1501.
[26] N. Sakai, T. Kawada, H. Yokokawa and M. Dokiya, J. Ceram. Soc. Jpn., 101 (1993) 1195.
[27] P. Sujatha Devi and M. Subba Rao, Thermochim. Acta, 15 (1989) 181.
[28] B.G. Tilset, H. Fjellvåg and A. Kjekshus, Acta Chem. Scand., submitted.
[29] P. Lacorre, J.B. Torrance, J. Pannetier, A.I. Nazzal, P.W. Wang and T.C. Huang, J. Solid State Chem., 91 (1991) 225.
[30] P. Bezdicka, A. Wattiaux, J.C. Grenier, M. Pouchard and P. Hagenmuller, Z. Anorg. Allg. Chem., 619 (1993) 7.
[31] J.L.G. Fierro and L.G. Tejuca, J. Catal., 87 (1984) 126.
[32] M. Seppänen, M. Kytö and P. Taskinen, Scand. J. Metall., 9 (1980) 3.
[33] K. Kamata, T. Nakajima, T. Hayashi and T. Nakamura, Mater. Res. Bull., 13 (1978) 49.
[34] M. Crespin, P. Levitz and L. Gatineau, J. Chem. Soc. Faraday Trans., 79 (1983) 1181.
[35] M. Seppänen, M. Kytö and P. Taskinen, Scand. J. Metall., 8 (1979) 199.
[36] C.N.R. Rao, J. Gopalakrishnan, K. Vidyasagar, A.K. Ganguli, A. Ramanan and L. Ganapathi, J. Mater. Res., 1 (1986) 280.
[37] N. Sakai and H. Fjellväg, to be published.